Electronic Supplementary Material (ESI) for Inorganic Chemistry Frontiers.

Supporting Information for

Ultra-low Ru Doped MOF-derived Hollow Nanorods for Efficient Oxygen Evolution Reaction

Dongmei Liu [a], Cheng Wang [a], Zhengming Zhou [c], Changqing Ye *[b], Rui Yu [a], Caiqin Wang *[d], Yukou Du *[a]

[a] *College of Chemistry, Chemical Engineering and Materials Science, Soochow University, 199 Renai Road, Suzhou 215123, P.R. China.*

[b] *Jiangsu Key Laboratory for Environmental Functional Materials, Institute of Chemistry, Biology and Materials Engineering, Suzhou University of Science and Technology, Suzhou 215009, PR China.*

[c] *West China School of Public Health and West China Fourth Hospital, Sichuan University, Chengdu, Sichuan, 610041, PR China.*

[d] *College of Science, Nanjing Forestry University, Nanjing 210037, PR China.*

** Corresponding authors: Tel: 86-512-65880089, Fax: 86-512-65880089;*

E-mail: yechangqing@mail.usts.edu.cn (C. Ye); wangcaiqin@njfu.edu.cn (C. Wang); duyk@suda.edu.cn (Y. Du)

Table of contents

Experimental Sections

Synthesis of Co precursor nanorod

The Co precursor nanorods were synthesized following the previously reported method.[1] Typically, 1.0 g of polyvinylpyrrolidone (PVP) and 0.64 g of cobalt (II) acetate tetrahydrate were dissolved in 200 mL of ethanol at room temperature to form a pink transparent solution. The above solution was refluxed under magnetic stirring at 85 ^{o}C for 2 h and cooled to room temperature. Afterwards, the pink precipitate was collected by centrifugation at 4000 rpm, washed with ethanol for 6 times to remove PVP and dried under vacuum for 12 h.

Synthesis of Co-MOF-74 (Co-MOF) hollow nanorods

The hollow Co-MOF-74 (denoted as Co-MOF) was prepared based on the Co precursor synthesized before. Firstly, 0.118 g of 2,5-dihydroxyterephthalic acid (H_4DOBDC) was dissolved in 30 mL N,N-dimethylformamide (DMF) as solution A, 0.1 g Co precursor was dissolved in 20 mL DMF as solutin B. Solution A was preheated to 85 ^{o}C in the oil bath and quickly poured into solutin B, then the resulting mixture was refluxed under magnetic stirring at 85 ^{o}C for 2 h. The formed Co-MOF hollow nanorods were then

collected by centrifugation, washed with DMF for several times and dispersed in 80 mL of methanol, heated at 50 ^{o}C for 6 h to remove DMF, the orange precipitate was centrifuged and washed with methanol for several times, and dried under vacuum for 12 h.

Synthesis of CoFe-MOF hollow nanorods

For the preparation of CoFe-MOF-2, 12 mg of the as-prepared Co-MOF was dispersed in 1 mL of ethanol as solution C, 6 mg of iron (II) chloride tetrahydrate was dissolved in the mixture of 5 mL deionized (DI) water and 5 mL of ethanol as solution C. Then, at room temperature, solution C was mixed with solution D rapidly and aged for 1 h. The dark green precipitate was centrifuged and washed with ethanol for three times and subsequently dried under vacuum. The synthetic processes of CoFe-MOF-1 and CoFe-MOF-3 are similar to CoFe-MOF-2, except that the amount of iron (II) chloride tetrahydrate was changed to be 12 mg (for CoFe-MOF-1) and 4 mg (for CoFe-MOF-3).

Synthesis of CoFe/D-MOF and Ru@CoFe/D-MOF

For the preparation of CoFe/D-MOF-2, 1 mL of fresh $NaBH_4$ solution (0.715 M) was dropped into 12 mg of CoFe-MOF-2 (in 5 mL of ethanol) under magnetic agitation, after stirring for 15 min, the dark orange precipitate was centrifuged, washed with ethanol for three times, then dried under vacuum. Afterwards, Ru@CoFe/D-MOF-2 (marked as Ru-2@CoFe/D-MOF-2) was prepared by adding 800 μL (2 mg/mL) of aqueous ruthenium(III) chloride into 8 mg of the CoFe/D-MOF-2 (in 5 mL DI water) and react for 24 h at room temperature, Ru-1@CoFe/D-MOF-2, Ru-3@CoFe/D-MOF-

2, Ru-4@CoFe/D-MOF-2 were synthesized by changing 800 μL of aqueous ruthenium(III) chloride into 500 μL, 1 mL and 1.5 mL.

Characterizations

Low-magnification transmission electron microscopy (TEM) was performed on a HITACHI HT7700 at 120 kV. High-angle annular dark-field scanning transmission electron microscopy (HAADF-STEM) and high-resolution TEM (HRTEM) was recorded on a FEI TecnaiG2F2 FEI Talos F200X S/TEM with a field-emission gun at 200 kV. Scanning electron microscopy (SEM) was conducted on a Hitachi S-4700 instrument operated at 15 kV under high vacuum. X-ray diffractometers (XRD) was carried out by Bruker D8 ADVANCE with Cu Kα radiation. The atomic ratio of Fe, Co and Ru was determined by Energy-dispersive X-ray (EDX) spectroscopy and Inductively coupled plasma-optical emission spectroscopy (ICP-OES) which conducted on Hitachi S-4700 instrument (15 kV) and VARIAN 710-ES, respectively. The electron spin resonance (ESR) was conducted on JES-X320 spectrometer at room temperature. The chemical states of CoFe-MOF-2, CoFe/D-MOF-2 and Ru@CoFe/D-MOF-2 were illustrated by X-ray photoelectron spectroscopy (XPS) performed on a VG scientific ESCA Lab 220 XL electron spectrometer using 300 W Al Kα radiation.

Electrochemical measurement

The measurements for water splitting were performed on CHI 660E electrochemical analyzer (Chenhua, Shanghai) in 1 M KOH. A three-electrode system was applied for OER tests, in which glassy carbon electrode (GCE) (diameter: 5 mm), graphite rod and saturated Ag/AgCl electrode were served as working electrode, counter electrode and reference electrode respectively. 5 mg catalysts were obtained by mixing the products with carbon powder (mass ratio =1:1). Then, 1 mL ethanol and 10 μL 5 wt% Nafion

solution were added into the as-prepared mixed catalysts, after 30 min of ultrasonic treatment, 10 μL of the ink was carefully deposited on GCE and dried naturally.

The reference potentials were transformed into the reversible hydrogen electrode (RHE) referring to the formula: E_{RHE} = E (Ag/AgCl) + 0.059 * pH + 0.197 V, the overpotential (η) was calculated by $\eta = E_{RHE}$ - 1.23 V. The linear sweep voltammetry (LSV) was conducted with scanning rate of 5 mV s^{-1}. The Tafel plots were obtained following the equation: $\eta = a + b \lg j$, where j means current density, and b represents Tafel slope. Non-faradic region was selected to perform Cyclic voltammetry (CV) measurements with scanning rates of 10 mV s^{-1} to 50 mV s^{-1}. The electrochemical impedance spectroscopy (EIS) tests were performed with the frequency ranging from 0.01 to 100 kHz. Notably, all the relevant electrochemical measurements were conducted without iR-correction.

Supporting Figures and Tables

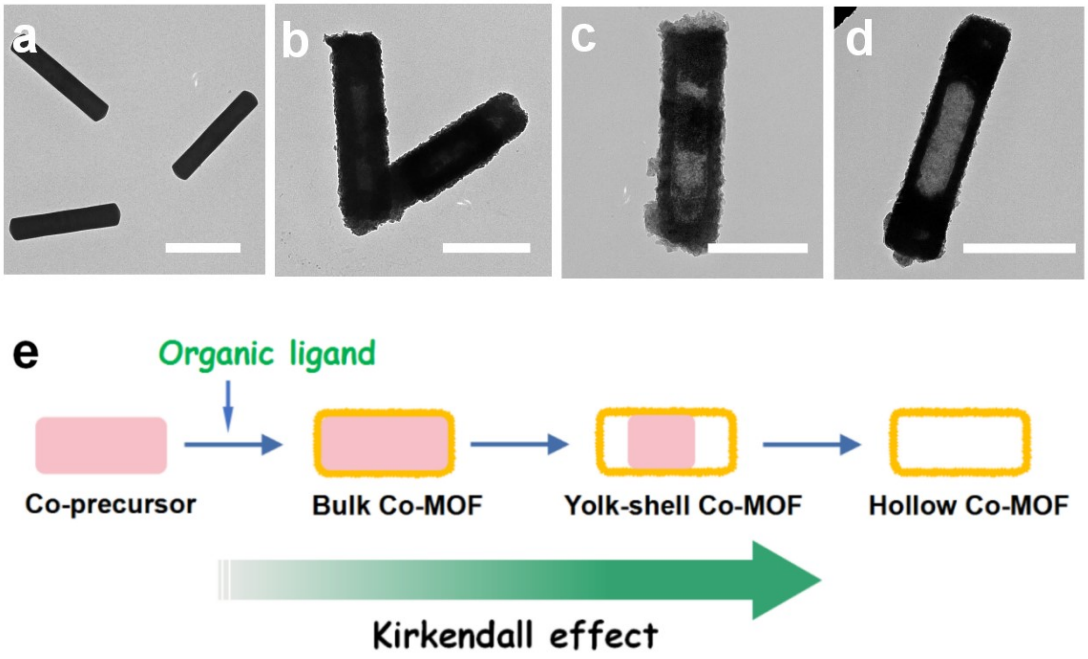

Fig.S1 TEM images of (a) Co precursor, (b-d) Co-MOF with reaction time prolonged. (e) Schematic diagram for the formation process of hollow Co-MOF nanorods and corresponding kirkendall effect . Scale bars are 1.0 μm in (a-d) .

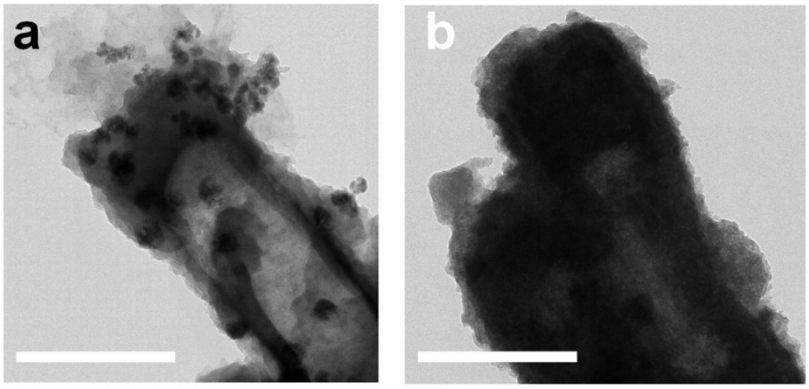

Fig.S2 TEM images of (a) CoFe/D-MOF-1 and (b) CoFe/D-MOF-3. Scale bars are 500 nm in (a-b).

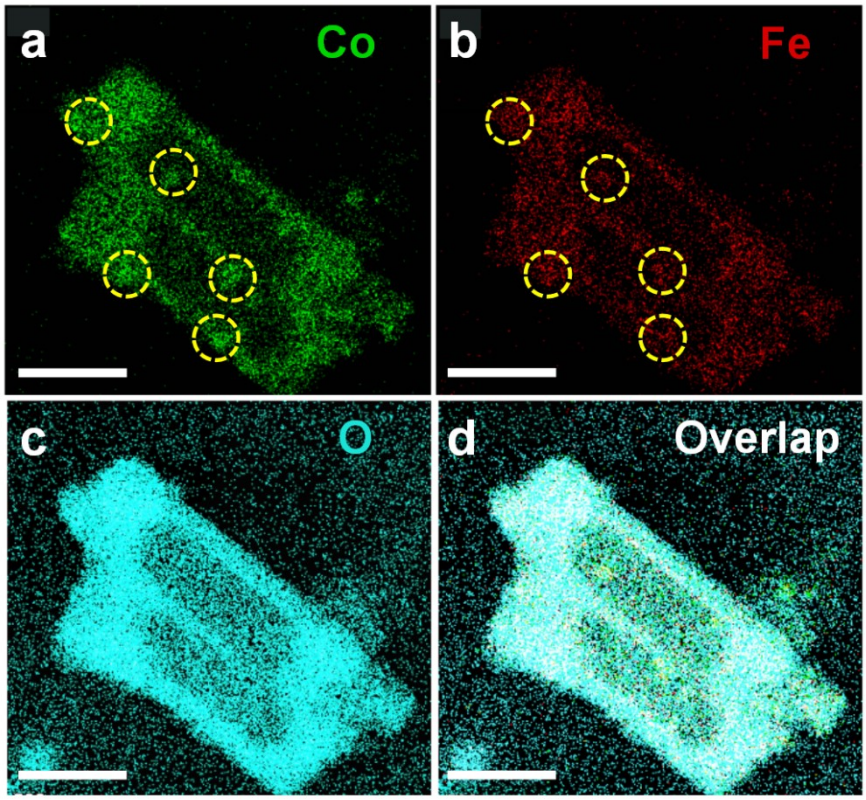

Fig.S3 EDS element mapping images of Co, Fe and O in CoFe/D-MOF-2 with scale bars of 500 nm.

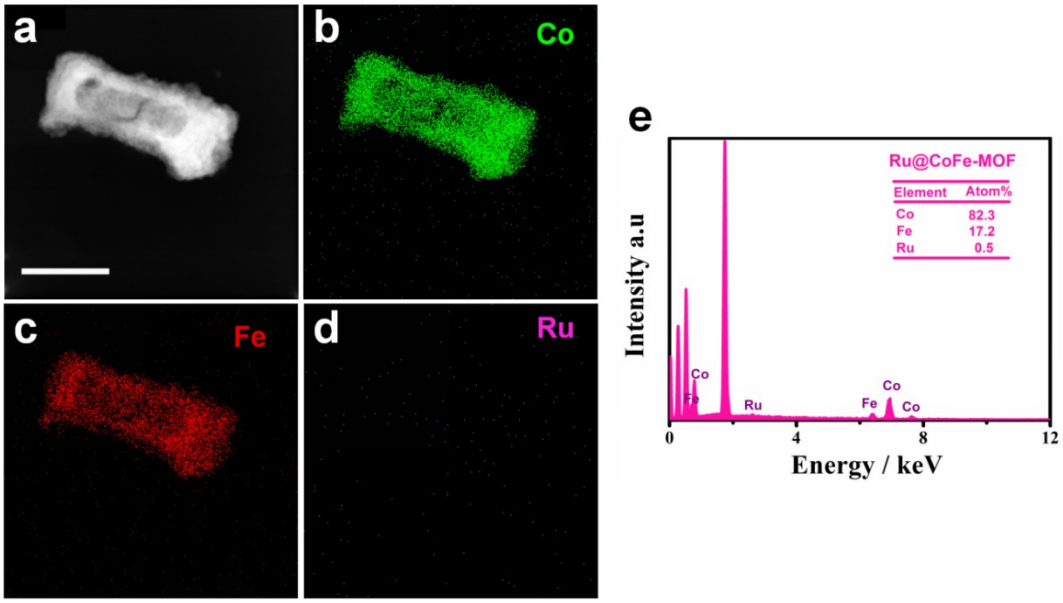

Fig.S4 (a) HAADF-STEM and (b-d) elemental mapping images of Ru@CoFe-MOF. Scale bars are 500 nm in (a-d). (e) EDS results of Ru@CoFe-MOF.

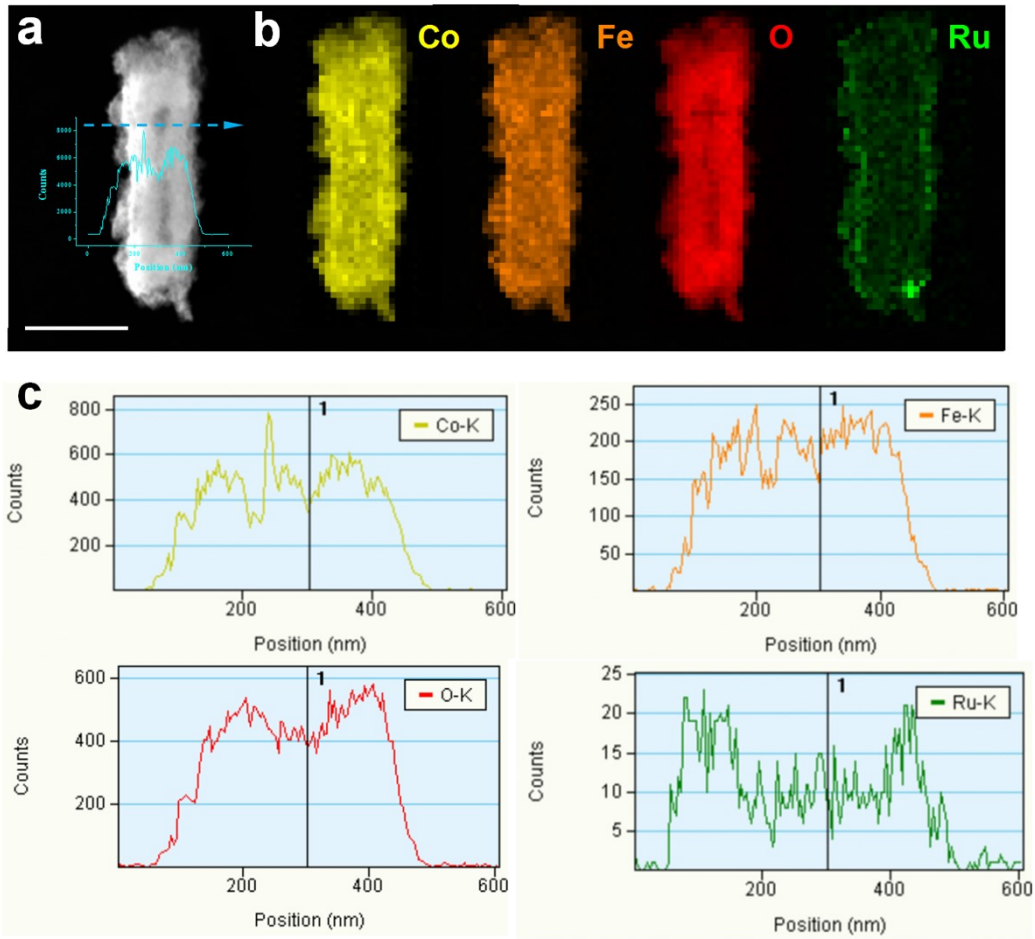

Fig.S5 (a) HAADF-STEM, (b) elemental mapping images and (c) corresponding EDS line scans of Ru@CoFe/D-MOF after electrolysis. Scale bar is 500 nm.

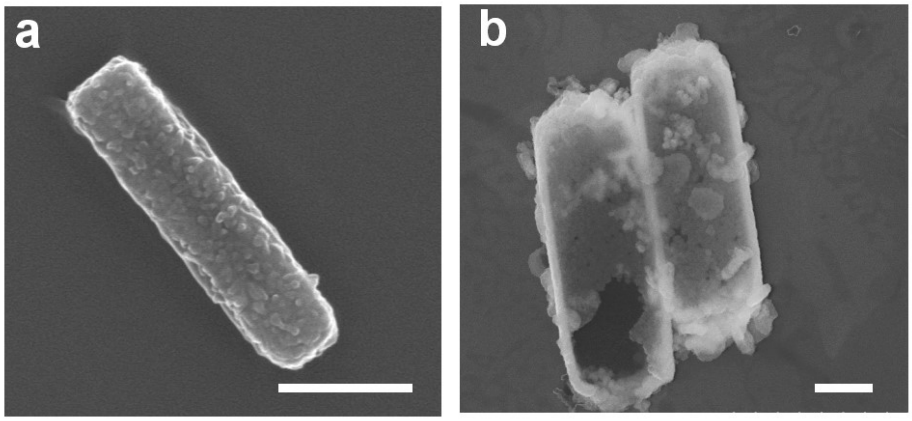

Fig.S6 SEM images of (a) Co-MOF and (b) Ru@CoFe/D-MOF. Scale bars are: 500 nm in (a) and 200 nm in (b).

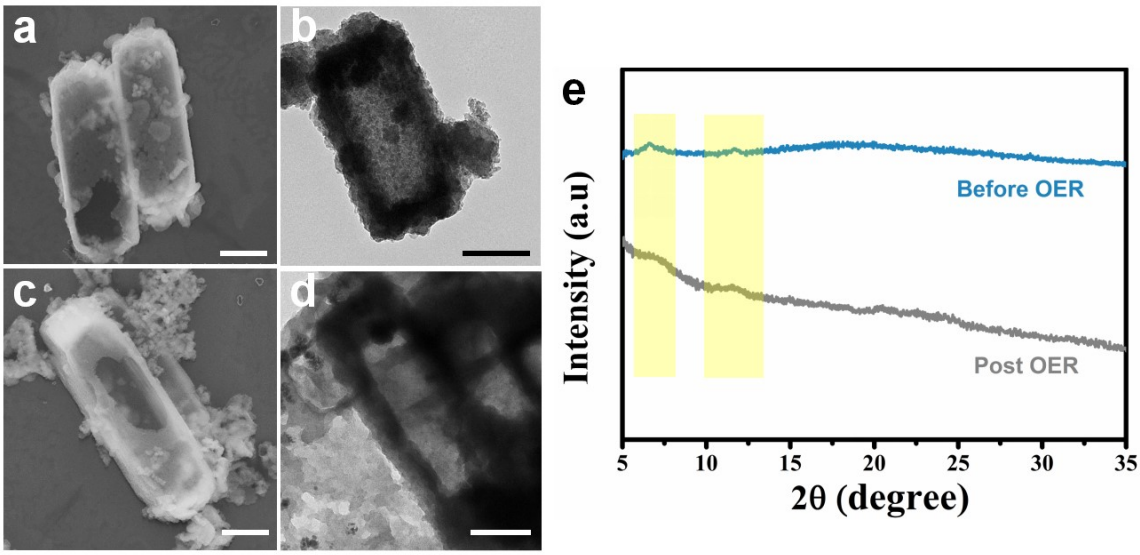

Fig.S7 SEM and TEM images of Ru@CoFe/D-MOF before (a, b) and after (c, d) stability test. (e) XRD patterns of initial CoFe/D-MOF (blue curve) and Ru@CoFe/D-MOF (gray curve) after electrochemical stability test. Scale bars: 200 nm in (a-d).

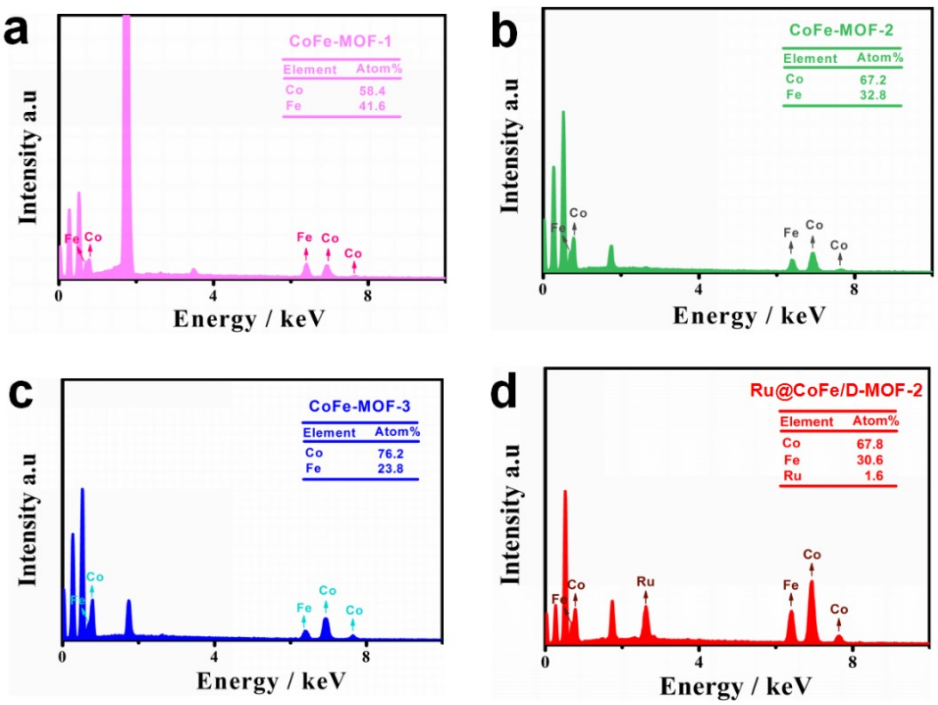

Fig.S8 Energy dispersive X-ray spectroscopy (EDS) of (a-c) CoFe-MOF with different mass ratio of Co/Fe, (d) Ru@CoFe/D-MOF-2.

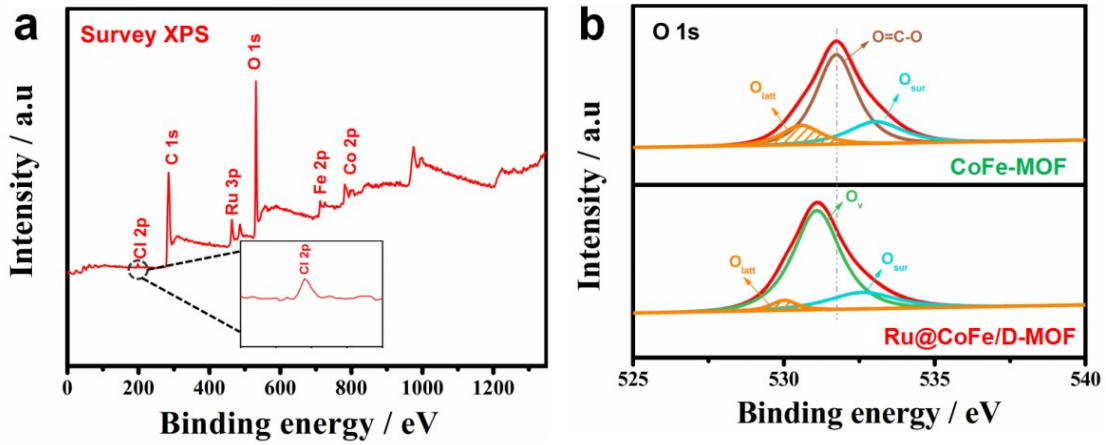

Fig.S9 (a) Survey XPS of Ru@CoFe/D-MOF-2, (b) O 1s region for CoFe-MOF-2 and Ru@CoFe/D-MOF-2.

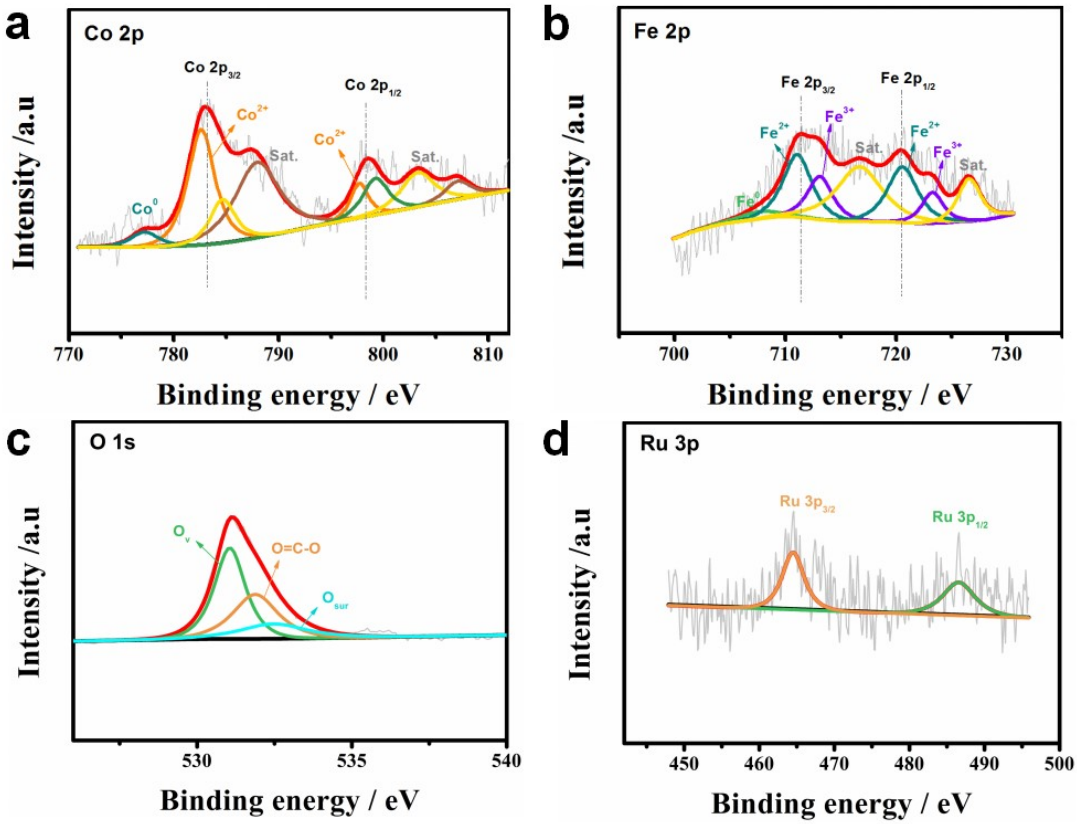

Fig.S10 High-resolution XPS results of (a) Co 2p, (b) Fe 2p, (c) O 1s and (d) Ru 3p regions for Ru@CoFe/D-MOF after electrochemical stability test.

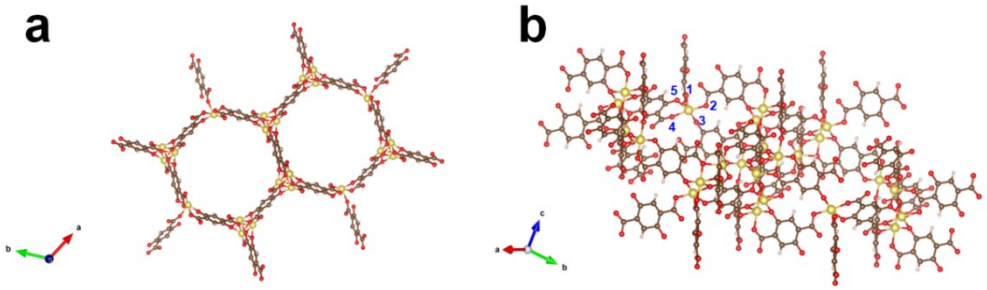

Fig.S11 Structure of Co-MOF observed from different orientation (a) top view and (b) side view. Color codes: Co:yellow, O:red, C: brown.

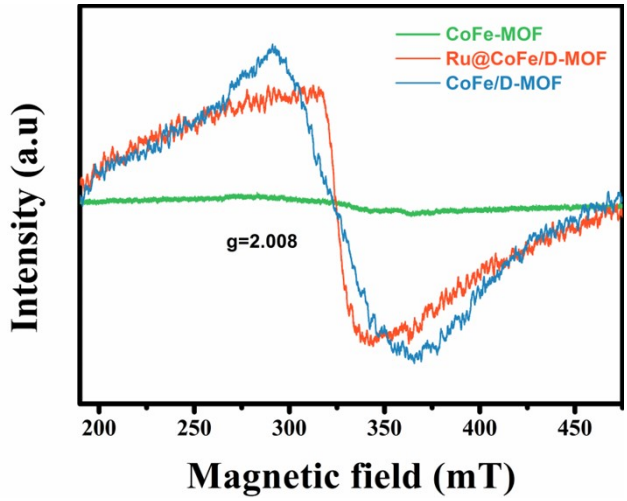

Fig.S12 ESR spectrum of CoFe-MOF, CoFe/D-MOF and Ru@CoFe/D-MOF. Preparation conditions: solid CoFe-MOF, CoFe/D-MOF and Ru@CoFe/D-MOF catalysts, room temperature.

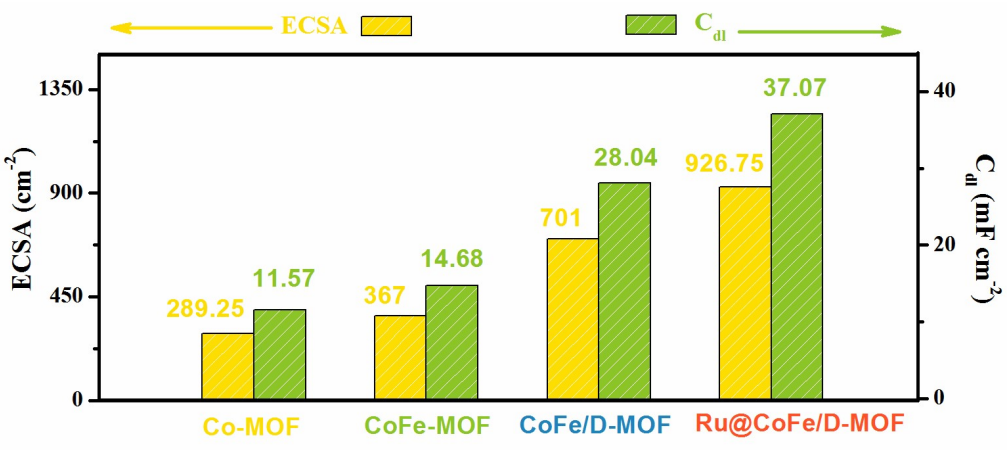

Fig.S13 ECSA and C_{dl} values of Co-MOF, CoFe-MOF-2, CoFe/D-MOF-2 and Ru@CoFe/D-MOF-2.

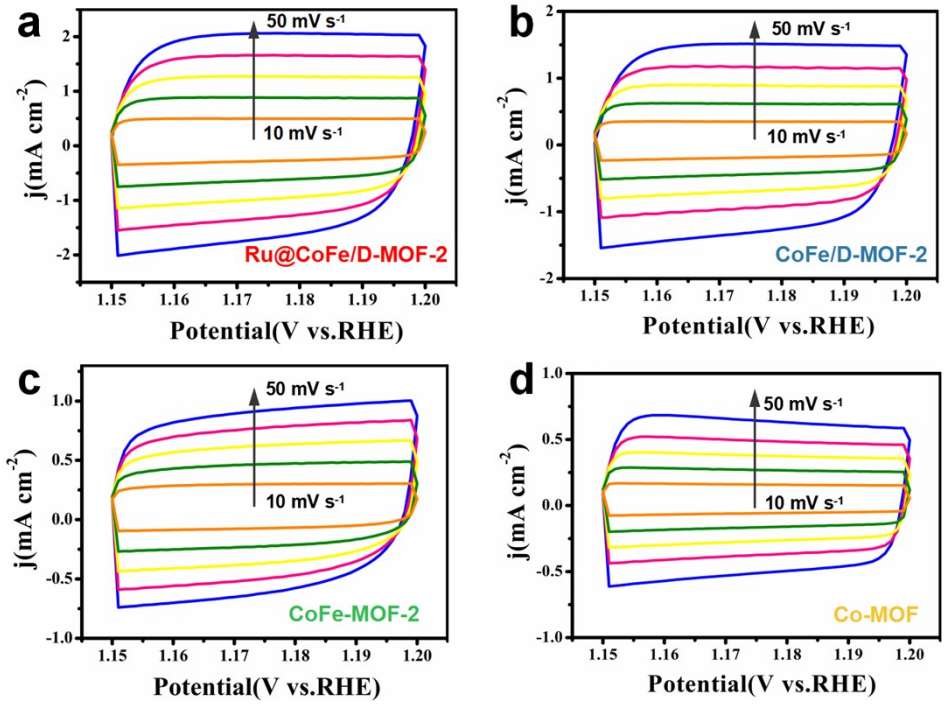

Fig.S14 CV curves of Ru@CoFe/D-MOF-2, CoFe/D-MOF-2, CoFe-MOF-2 and Co-MOF from scan rates of 10 mV s^{-1}~50 mV s^{-1}.

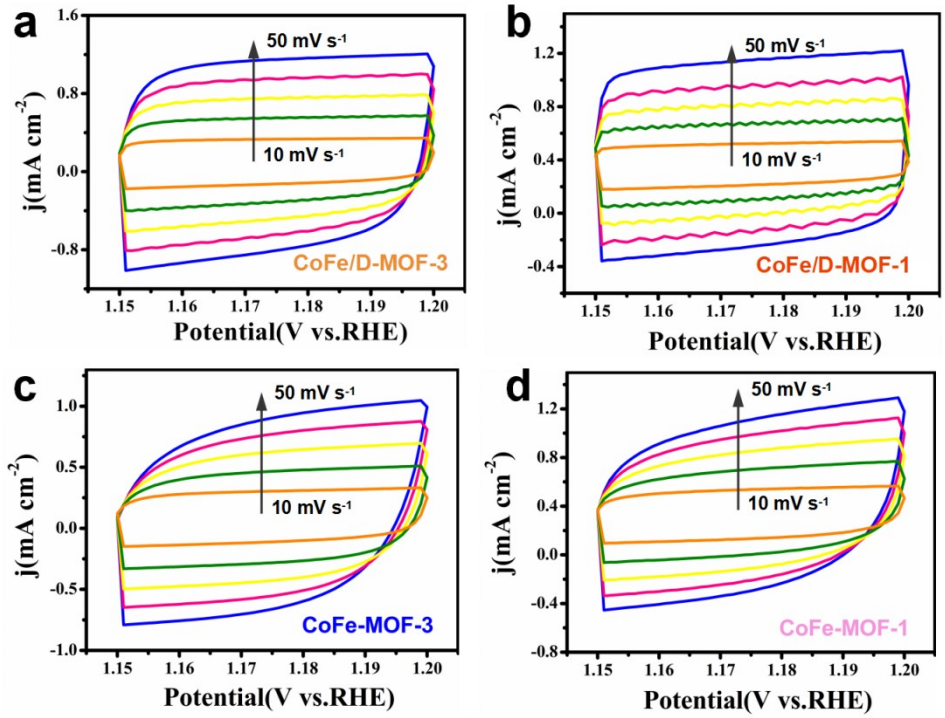

Fig.S15 CV curves of CoFe/D-MOF-3, CoFe/D-MOF-1, CoFe-MOF-3 and CoFe-MOF-1 from scan rates of 10 mV s^{-1}~50 mV s^{-1}.

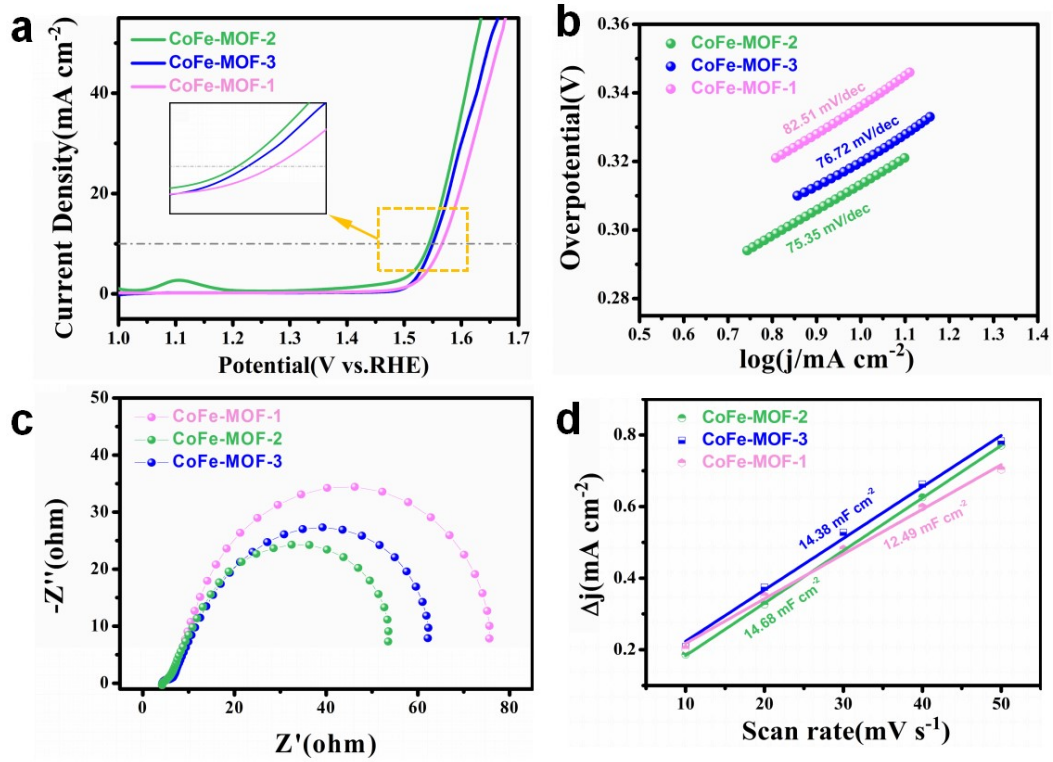

Fig.S16 (a) LSV polarization curves of CoFe-MOF with different mass ratio of Co:Fe. (b) Corresponding Tafel plots. (c) EIS results. (d) Plots of current density vs. scan rate obtained by non-faradic CV scanning.

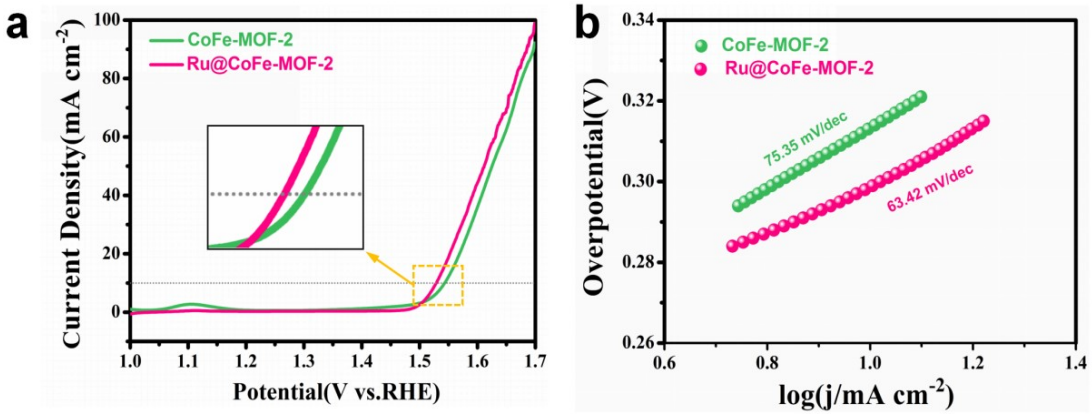

Fig.S17 (a) LSV polarization curves of CoFe-MOF-2 and Ru@CoFe-MOF-2 in 1 M KOH. (b) Corresponding Tafel plots.

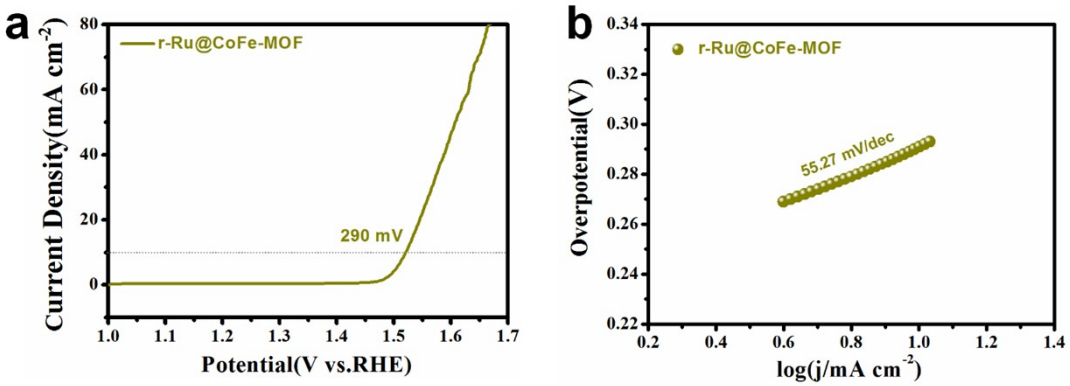

Fig.S18 (a) LSV polarization curves and (b) Corresponding Tafel plots of r-Ru@CoFe-MOF.

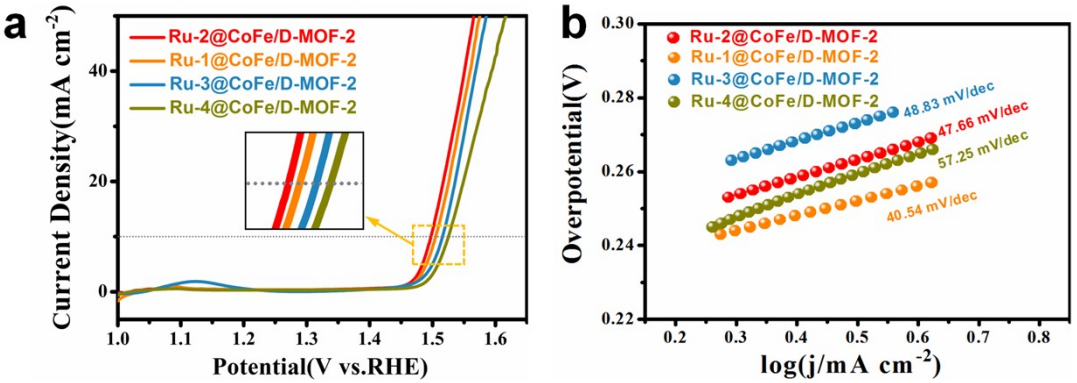

Fig.S19 (a) LSV polarization curves of Ru-1@CoFe/CoFe-MOF-2, Ru-2@CoFe/CoFe-MOF-2, Ru-3@CoFe/CoFe-MOF-2, Ru-4@CoFe/CoFe-MOF-2 in 1 M KOH. (b) Corresponding Tafel plots.

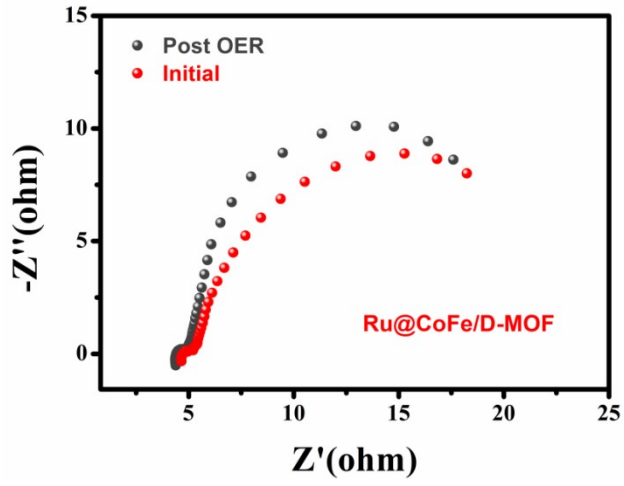

Fig.S20 Nyquist plots of Ru@CoFe/D-MOF before and after OER stability test. (gray

dots: after durability test, red dots: before durability test)

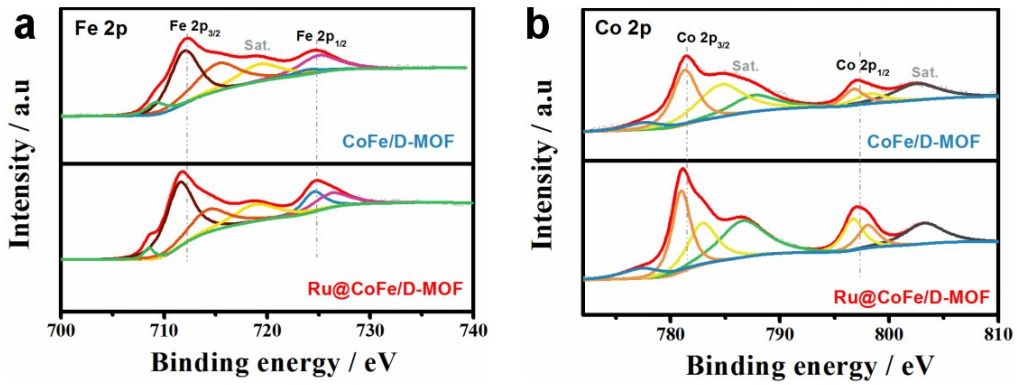

Fig.S21 High-resolution XPS results of (a) Co 2p and (b) Fe 2p regions for CoFe/D-MOF and Ru@CoFe/D-MOF.

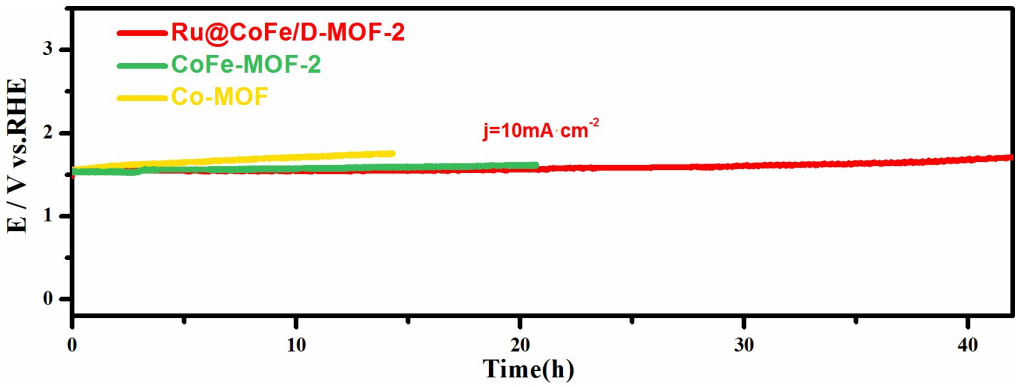

Fig.S22 Chronopotentiometric curves of Ru@CoFe/D-MOF-2, CoFe-MOF-2 and Co-MOF at current density of 10 mA cm^{-2}.

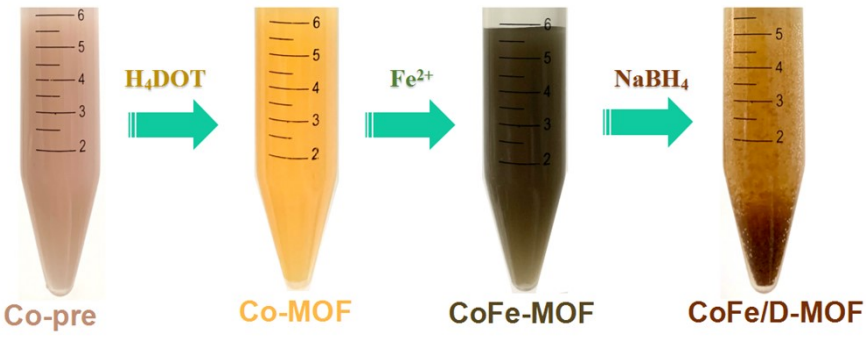

Fig.S23 Photos of the suspension of Co precursor (Co-pre), Co-MOF, CoFe-MOF and

CoFe/D-MOF.

Table S1 Summary of various Ru-doped and CoFe-based catalysts for OER in alkaline media.

Catalyst	Overpotential (mV) at 10 mA cm^{-2}	Tafel slope ($mV\ dec^{-1}$)	Reference
Ru@CoFe/D-MOF-2	**265**	**37.07**	**This work**
RuRhCo	324	147	[2]
FeCoSe@NCNS	320	82.3	[3]
$RuNi_1Co_1$@CMT	299	83	[4]
Ru-CoP/NC	330	65	[5]
Ru-FeRu@C/NC	345	64.7	[6]
$Ru_{0.7}Co_{0.3}$ aerogel	272	41.6	[7]
M_2Ru_1O	266	73.45	[8]
Ru@Bpy-POP	270	67	[9]
Co_xFe_{1-x}-MOF-74	280	56	[10]
P-Co_3O_4	283	85.3	[11]
α-Fe_2O_3	305	51.8	[12]
CoFe-LDH/GF	252	61	[13]
Co_8Fe_1-LDH	262	42	[14]
$Co_2NiS_{2.4}(OH)_{1.2}$	279	52	[15]

Table S2 ICP data for Co, Fe, Ru contents in different samples.

Sample	Co (at%)	Fe (at%)	Ru (at%)
Ru@CoFe/D-MOF	70.2	28.3	1.5
Ru@CoFe-MOF	78.3	21.1	0.6
CoFe-MOF-1	55.3	44.7	--

CoFe-MOF-2	68.7	31.3	--
CoFe-MOF-3	75.9	24.1	--

References

1. L. Yu, J. F. Yang, X. W. Lou, Formation of CoS_2 nanobubble hollow prisms for highly reversible lithium storage, *Angew. Chem. Int. Ed*, 2016, **55**, 13422-13426.

2. Y. Cui, Z. Xu, D. Chen, T. Li, H. Yang, X. Mu, X. Gu, H. Zhou, S. Liu, S. C. Mu, Trace oxophilic metal induced surface reconstruction at buried RuRh cluster interfaces possesses extremely fast hydrogen redox kinetics, *Nano Energy*, 2021, **90**, 106579.

3. Y. Pan, M. Wang, M. Li, G. Sun, Y. Chen, Y. Liu, W. Zhu, B. Wang, In-situ construction of N-doped carbon nanosnakes encapsulated FeCoSe nanoparticles as efficient bifunctional electrocatalyst for overall water splitting, *J. Energy. Chem*. 2022, **68**, 699-708.

4. Y. Xue, Q. Yan, X. Bai, Y. Xu, X. Zhang, Y. Li, K. Zhu, K. Ye, J. Yan, D. Cao, G. Wang, Ruthenium-nickel-cobalt alloy nanoparticles embedded in hollow carbon microtubes as a bifunctional mosaic catalyst for overall water splitting, *J. Colloid, Interf. Sci*. 2022, **612**, 710-721.

5. Y. R. Hao, H. Xue, J. Sun, N. Guo, T. Song, J. Sun, Q. Wang, Tuning the Electronic Structure of CoP Embedded in N-Doped Porous Carbon Nanocubes Via Ru Doping for Efficient Hydrogen Evolution, *ACS Appl. Mater. Interfaces*. 2021, **13**, 56035-56044.

6. W. Feng, Y. Feng, J. Chen, H. Wang, Y. Hu, T. Luo, C. Yuan, L. Cao, L. Feng, J. Huang, Interfacial electronic engineering of Ru/FeRu nanoparticles as efficient

trifunctional electrocatalyst for overall water splitting and Zn-air battery, *Chem. Eng. J.*, 2022, **437**, 135456.

7. Z. Lin, S. Liu, Y. Liu, Z. Liu, S. Zhang, X. Zhang, Y. Tian, Z. Tang, Rational design of Ru aerogel and RuCo aerogels with abundant oxygen vacancies for hydrogen evolution reaction, oxygen evolution reaction, and overall water splitting, *J. Power. Sources*., 2021, **514**, 230600.

8. F. Zhu, J. Xue, L. Zeng, J. Shang, S. Lu, X. Cao, B. F. Abrahams, H. Gu, J. Lang, One-pot pyrolysis synthesis of highly active Ru/RuO_x nanoclusters for water splitting, *Nano Res*, 2021, 15, 1020-1026.

9. B. Boro, M.K. Adak, S. Biswas, C. Sarkar, Y. Nailwal, A. Shrotri, B. Chakraborty, B. M. Wong, J. Mondal, Electrocatalytic water oxidation performance in an extended porous organic framework with a covalent alliance of distinct Ru sites, *Nanoscale*, 2022, **14**, 7621-7633.

10. X. Zhao, B. Pattengale, D. Fan, Z. Zou, Y. Zhao, J. Du, J. Huang, C. Xu, Mixed-node metal-organic frameworks as efficient electrocatalysts for oxygen evolution reaction, *ACS Energy Lett*, 2018, **3**, 2520-2526.

11. D. Song, J. Sun, L. Sun, S. Zhai, G.W. Ho, H. Wu, W.Q. Deng, Acidic media regulated hierarchical cobalt compounds with phosphorous doping as water splitting Electrocatalysts, *Adv. Energy. Mater*, 2021, **11**, 2100358.

12. H. Wu, T. Yang, Y. Du, L. Shen, G.W. Ho, Identification of facet-governing reactivity in hematite for oxygen evolution, *Adv. Mater*, 2018, **30**, e1804341.

13. B. Deng, J. Liang, L. Yue, T. Li, Q. Liu, Y. Liu, S. Gao, A.A. Alshehri, K.A. Alzahrani, Y. Luo, X. Sun, CoFe-LDH nanowire arrays on graphite felt: A high-performance oxygen evolution electrocatalyst in alkaline media, *Chinese Chem Lett*, 2022, **33**, 890-892.

14. J. Zhao, X.-R. Wang, F.-W. Chen, C. He, X.-J. Wang, Y.-P. Li, R.-H. Liu, X.-M. Chen, Y.-J. Hao, M. Yang, F.-T. Li, A one-step synthesis of hierarchical porous CoFe-layered double hydroxide nanosheets with optimized composition for enhanced oxygen evolution electrocatalysis, *Inorg. Chem. Front*., 2020, **7**, 737.

15. B. Wang, C. Tang, H.-F. Wang, X. Chen, R. Cao, Q. Zhang, Core-branch CoNi hydroxysulfides with versatilely regulated electronic and surface structures for superior oxygen evolution electrocatalysis, *J. Energy. Chem*., 2019, **38**, 8-14.

A